High resolution, dynamic imaging of early mouse and human liver bud morphogenesis in three dimensions

Tala Mon,[1], Ogechi Ogoke[1], Claire Shamul[1], Shatoni Ross[1] Saroja Rao[3], Natesh Parashurama [1,2,6 *]

[1] Department of Chemical and Biological Engineering, University at Buffalo (State University of New York), Furnas Hall, Buffalo, NY 14260

[2] Clinical and Translation Research Center (CTRC), University at Buffalo (State University of New York), 875 Ellicott St., Buffalo, NY 14203

[3] Department of Biological Sciences, University at Buffalo (State University of New York), College of Arts and Sciences, 109 Cooke Hall, Buffalo, NY 14260-4610

[6] Department of Biomedical Engineering, University at Buffalo (State University of New York), Furnas Hall, Buffalo, NY 14260

* Corresponding Author

Running Title: Imaging 3D liver bud morphogenesis

Keywords: liver development, liver imaging, liver organogenesis, hepatic cords, liver bud, septum transversum mesenchyme

Contact information:
Natesh Parashurama MD PhD, 907 Furnas Hall, Buffalo, NY 14260; Tel: 716-645-1201; Fax: 716-645-3822; e-mail: nateshp@buffalo.edu

ABSTRACT

Liver organogenesis has thus far served as a paradigm for solid organ formation, and has recently attracted interest due to challenges faced in liver regenerative medicine. Murine genetic studies indicate that early steps in morphogenesis are required, suggesting that three-dimensional imaging of early liver morphogenesis at high resolution can improve our understanding. Unfortunately, existing approaches to image early liver morphogenesis have been unable to achieve high spatial resolution (1-5 um) required. In

this study, we focused on imaging, visualization, and analysis of early liver development. We utilized available online databases for both mouse (EMAP) and human (3D Atlas of Human Embryology) liver development. To visualize liver bud morphogenesis at high spatial resolution, we performed 3D reconstructions of stacked, digital tissue sections. We show dynamic 3D hepatic cord formation in the mouse in humans. Interestingly, when we quantified fetal liver growth, we showed that 3D fetal liver growth appears to occur in spurts rather continuously, and 3D images suggest that there could be considerable remodeling during these stages. Further, our analysis of the STM, in both mouse and humans, demonstrates that it increases in size during early fetal liver growth, that is highly interconnecting with liver epithelium, and that it can have strong local effects on growth. Finally, we identify and visualize and identify human hepatic cord formation followed by rapid sheet-like growth, which we propose could be an under-appreciated morphological feature that enables rapid growth of early human fetal liver. These studies will motivate future approaches to employ *in vitro* culture and organoid technology to improve human PSC differentiation, and improve disease modeling, and therapeutic opportunities for liver diseases. In conclusion, compared to 2D sectioning, high spatial resolution imaging of the mouse and human 3D liver bud morphogenesis enables greatly improved visualization of the hepatic cords, 3D sheet-like liver cell growth, STM-epithelial cell interactions, and quantitative comparisons between mouse and human liver bud morphogenesis.

INTRODUCTION

The wide-ranging, global epidemic of chronic end-stage liver disease has garnered increased interest in liver tissue engineering and liver regenerative medicine, including tools for hepatocyte (HEP) culture and expansion, stem cell biology of the liver, tissue chips to replace liver functions, *in vivo* disease modeling, and drug development (*1*). The expansion of liver research into these numerous directions has been sustained by fundamental and seminal studies of hepatic, biliary and vasculature development, reviewed elsewhere (*2*). These studies detail key molecular and morphogenetic steps in liver organogenesis development, which are intricately linked to the liver bud undergoing rapid and exponential fetal liver three dimensional (3D) growth, leading to the largest internal organ in the body. If these 3D morphogenetic steps can be further revealed through imaging, perhaps this can augment approaches towards directed differentiation of HEPs from stem cells and stem cell-derived organoids, disease modeling, and cell-based therapies.

Seminal genetic studies have established major stages of early liver bud morphogenesis as part of the liver organogenesis process, and the dynamic molecular underpinnings that drive these steps. The liver bud is a transient, multicellular structure that arises during E8.5 in mice and ~day 25 in humans, on

the scale of 100-200 µm in width and length (*3*). At E8.5, the liver bud contains the liver diverticulum, a ventral out-pocketing of the single cell-layered gut tube, surrounded by a layer of endothelial cells, which is then surrounded ventrally by the septum transversum mesenchyme (STM) (*3*). At E9.0, the epithelium within the gut tube transitions to a pseudostratified epithelium, and thickens in response to cardiac patterning of foregut endoderm via FGF2 (*4, 5*), STM patterning of hepatic endoderm via BMP4 (*6*), and endothelial cells patterning of adjacent foregut endoderm towards hepatic endoderm (*7*). These stages exhibit coupling between transcriptional (molecular) changes and cell fate. For example, Foxa2, the first known pioneer transcription factor, is upregulated in hepatic endoderm and primes silent liver genes within hepatic endoderm prior to overt morphogenesis (*8*), while Hex expression occurs during pseudostratification, prior to hepatic cord formation (*9*). Hepatic cord formation is a particularly critical cellular process, because the absence of hepatic cords leads to a severe stunting of liver growth and malformed hepatic sinusoids (*10*). These hepatic cords form at E9.5 (23-25 somite stage) and are defined as finger-like projections that protrude into the STM, express the master transcription factors Hex (*11*), Prox1 (*12*), and Tbx3 (*13*), and undergo both EMT (*14*) and collective cell migration (*15*). These genetic studies collectively demonstrate that hepatic cords form rapidly and have a short half-life. Despite their importance, existing histological studies demonstrate hepatic cords with a wide range of geometry, location, and thickness of the hepatic cords (*7, 16*). To our knowledge, the hepatic cords have not been imaged/visualized in 3D dimensions at high spatial resolution.

The various mesenchymal elements within the liver bud bear a large role in early 3D fetal liver growth and morphogenesis. The STM envelopes the early liver diverticulum in 3D and mediates growth by soluble factor-based induction, key signaling pathways, and transcriptional regulation. For example, genetic studies of BMP4, smad2/3 and neurturin (all part of the TGFß superfamily) (*17*), (*18*), HEP growth factor (HGF) (*19*), and ephrins (*20*) all demonstrate a role for the inductive properties of STM. Smad 2/3 (TGFß superfamily) haplo-deficient embryos exhibit severely disrupted liver growth by E14.5, due to both loss of ß1-integrin (a known TGFß, target) expression, and mislocalized E-cadherin expression (*17*). HGF knockout studies are mediated by a lack of c-met receptor engagement in hepatoblasts (*19*). Further, GATA4 -/- embryos lack STM, hepatic cord formation, and subsequent liver development (*21*). Knockout of Hlx1, which is strongly expressed within the STM, does not affect early liver specification and hepatic cord formation, but greatly affects 3D liver expansion (*22*). Finally, ARF6 knockout disrupts cell membrane polarization, and receptor recycling in liver epithelia (*16*). In addition to the STM, hematopoietic stem cells, which seed the fetal liver at ~E11.0, and 5-6 weeks in human liver, play a role in liver growth. The absence of fetal liver hematopoiesis leads to complex liver morphological effects with mixed phenotypes (*23*), while affecting liver maturation via the cytokine oncostatin M (OSM) (*24*). Finally, endothelial cells within the developing sinusoids play a large role in inductive liver

growth (*25*). Supporting this, their absence in flk -/- mice inhibits liver growth, and *in vivo* studies of explanted mouse liver bud demonstrate that endothelial-lined, branched microvasculature induces 3D liver bud outgrowth even in the absence of blood flow (*7*). Moreover, VEGF-A, HGF, IL-6, and Wnt are collectively secreted from sinusoidal endothelial cells and signal to HEPs *in vivo* (*26*). Taken together, these studies convey the strong inductive, role mesenchyme in 3D fetal liver growth and organogenesis, although imaging/visualization of the STM in 3D has not been achieved.

Despite the significance of 3D liver morphogenesis, dynamic imaging of early liver bud morphogenesis has been challenging, and there is a need for high spatial resolution (~1-10 μm), dynamic (high temporal resolution), and small field of view imaging. Established techniques include immunohistochemistry, but this only enables 2D rather than 3D visualization of structure, is highly dependent upon tissue preparation and sectioning angle, and exhibits inter-subject variability (*7, 16*). To assess human fetal liver growth, scientists have used liver weights or liver morphometry (*27*), or noninvasive imaging approaches, like ultrasound (*28*), but these studies are not focused upon early liver bud morphogenesis. Noninvasive imaging of liver bud morphogenesis is challenging to perform *in utero* due to tissues, fluids, subject motion, and breathing artifacts. Nonetheless, noninvasive embryo imaging approaches(*29*) include light sheet microscopy, (*30*), ultrasound (*31*), optical coherence tomography (OCT) (*32*), computed tomography (CT) (*33*), magnetic resonance imaging (MRI) (*34*), and photoacoustic tomography (*34*), and we have recently summarized these imaging techniques (*35*). High resolution approaches like E11.5 mouse embryo CT (*33*) and optical projection tomography (*36*), while promising, have not imaged 3D liver bud morphogenesis. Overall, this establishes the need for new approaches that employ high spatial and temporal resolution imaging of the developing liver bud in 3D.

The E-mouse atlas project (EMAP) started with a concerted effort for 3D digital visualization of anatomy, histology, and gene expression during embryogenesis (*37*), and the 3D Atlas of Human Embryology project followed (*38*). We hypothesize that these digital resources could be used to better image and visualize early liver morphogenesis. Here, we used both the EMAP and the 3D Atlas of Human Embryology to more quantitatively image early liver bud morphogenesis. We performed 3D reconstructions of stacked, digital tissue sections of mouse and human liver, highlighting 3D hepatic cord formation, liver growth, STM-liver interactions, and sheet-like liver growth.

METHODS

Mouse liver development data visualization, three-dimensional reconstruction, and analysis

Aligned and registered image slices from each desired time point were downloaded from eMouseAtlas database and e-Mouse Atlas Project (EMAP, emouseatlas.org) (*37*) in WLZ format (*39*). The WLZ files

were developed from H&E stains of mouse embryos. Embryos were prepared by fixation, clearing, and embedded in wax, sectioned, stained and mounted on slides. Each time point was based on one specimen. Slices were converted to NII format which preserves the scaling of micrometers to pixels for import into ImageJ (https://imagej.nih.gov/). Specimens ranged from 244 to 869 slices with 4 μm per pixel in the x and y dimensions and 7 μm in the z dimension. Using Segmentation Editor, pre-tagged developing liver, septum transverse mesenchyme (STM), and the gut tube, were segmented arbitrarily into green, red, and yellow, respectively. E8.5 contained only pre-segmented areas of the liver diverticulum and gut tube, but not the STM. When needed, we estimated tissues boundaries, and colored then using the same approach, using existing textbooks and online resources of mouse and human developmental biology. (**Figure 1, Supplemental Figures 1-3**). 3D reconstruction of the existing liver bud was performed using the 3D data set which enables selection gut tube endoderm, hepatic endoderm, and STM. 3D imaging of the 3D reconstructed mouse liver bud within the whole embryo was unable to demonstrate effective images (**Figure 1, Supplemental Figure 1-3**). To focus the field of view to the liver bud only, the embryo was removed from view. When the STM or gut tube was obscuring the liver bud, the opacity of these tissues was reduced to 50%. Light and shading were at default settings and movies were recorded using the built-in tool of ImageJ 3D Viewer. Movies were created by 2 frames per degree of rotation and exported at 7 fps at a resolution of 512 x 512 pixels.

Human data and visualization

For the human development, grey image slices of the aligned and registered H&E stains are downloaded from the 3D Atlas of Human Embryology (3dembryoatlas.com) along with the label files (*40*). Each time point was based on one specimen. Grey and label files are imported into ImageJ using the TrakEM2 plugin and the scaling of micrometers to pixels is set using values provided by the authors. The STM was segmented manually and was readily apparent on histological sections, whereas for the developing liver and the gut tube we used the pre-existing segmentation. All segmented regions are exported as image stacks in TIFF format. 3D reconstruction was performed by importing the stacks into the 3D Viewer plugin with a smoothness factor of 10. Movies were created by 2 frames per degree of rotation and exported at 7 fps at a resolution of 512 x 512 pixels.

Calculation of volumes and surface area of embryonic structures

Using the 3D Manager plugin, volume and surface area were measured by through the Measure 3D option after loading the image stacks.

Estimation of cellular density in the gut tube, liver, and STM

For each region, the original histology was examined and imported into ImageJ. Random sections of each region were selected, and number of cells were counted. This count was divided by the area of the sections. It was assumed that the height of each cell was 10μm and further divided by a height estimation of 10 μm, to give a value of cells per cubic micron.

RESULTS

3D dynamic imaging of the liver epithelium during murine embryonic development.

To image the murine liver bud in 3D, we analyzed 3D reconstructions of stacked, digital, cleared, hematoxylin and eosin (H& E) tissue sections from mouse development at E8.5, E9, E9.5, and E10. In representative images from the E9.5 mouse, the liver bud epithelium (green) could be clearly delineated from the neighboring gut tube (yellow) and the surrounding STM (red) by tracing thickened liver epithelium, in the coronal (**Supplemental Figure 1A**) and sagittal directions (**Supplemental Figure 1B**). Representative images for E8.5, E9.0, and E10 are shown (**Supplemental Figures 2-4**). These segmented sections were reconstructed in 3D and imaged in whole embryo images (**Supplemental Figures 1C-F**). An increase in the liver bud between E8.5 to E10.0 can be observed based on the increase in overall embryo size (**Supplemental Figures 1C-F**). However, the liver epithelium cannot be visualized and the liver bud volumes appear grossly similar (**Supplemental Figures 1C-F**).

Next, we reduced the field of view and engineered images of only the 3D liver bud epithelium, STM, and gut tube. Initially, the E8.5 liver epithelium appears as a sheet of cells in the shape of a triangle, with the apex in the cranial side, a base of 25 μm, and a height of 30 μm (**Figure 1A**). Rotation of the E8.5 3D images indicate both tube-like regions and flat sheet-like regions, perhaps indicative of both the squamous (sheet) and cuboidal epithelium within the gut tube endoderm (*41*) (**Supplemental Figure 5, Supplemental Video 1-2**). The E8.5 liver bud is on the order of 50-100 μm x 50-100 μm x 10 μm (thickness), which we estimate to be only 250-500 cells initially. Interestingly, our data suggests that the hepatic endoderm cell sheet curves forward to make a near 90^{o} angle (**Supplemental Figure 5, Supplemental Video 1**). Upon closure of the gut tube at E9.0, the liver bud has grown with an elliptical shape (**Figure 1B**), and between E9.0 and E10.0, the liver bud undergoes remodeling with the elliptical long axis in the cranial-caudal direction (long axis of 300 μm), versus the lateral direction (**Compare Figures 1B, 1C, and 1D**).

Imaging of migrating cords and sheet-like growth in the developing mouse liver bud.

Our goal was to visualize the hepatic cords in 3D. When performing 3D analysis by rotation of the E9.0 liver bud, we observed numerous miniature finger-like projections with dimensions of 1-10μm in length/diameter, better visualized in video format (**Figure 3A-B, Supplementary Video 2**). Interestingly,

we also observed sheet-like growth, arranged in a series of ridges, at E9.0, from the superior to the inferior portion of the liver bud (**Figure 3C**, **Supplementary Video 2).** Similar but slightly larger finger-like projections are observed in at E9.5 (5-10 μm) (**Figure 3D-E, Supplementary Video 3**), indicating 3D growth. We again observed sheet-like 3D growth arranged in larger ridges at E9.5 compared to E9.0 (**Figure 3E, Supplementary Video 3**). It is known that hepatic cords extend into the STM, and that at later times, the STM, hepatic cords, and endothelial cells intermingle. We assumed that when we can no longer observe the STM (no longer can be segmented), the STM cells were intermingled with hepatoblasts, and this occurred by E10.0 3D reconstruction of E10 murine liver bud demonstrates numerous interconnections of hepatic cords that form a sponge-like, trabeculated tissue (**Figure 3F-H, Supplementary Video 3**). Interestingly many more finger-like projections are present, observed in multidirectional, lateral, and caudal-cranial direction (**Figures 3F-H, Supplementary Videos 4 and 5**). Further, trabeculation can be viewed inside the liver, best illustrated by video at E10.0 (**Figure 4H, Supplementary video 5**), in which surfaces that appear green and enclosed, are actually the empty voids, devoid of any cells. Overall, we observe hepatic cords and a sheet-like growth pattern at E9.0-9.5, and further hepatic cord formation and trabeculation by E10.

Quantification of murine liver bud volumes and surface area

To quantify volume of mouse liver bud during growth, the absolute liver bud volumes of 3D reconstructed liver bud and embryo were measured. We observed a 3.75 x 10^3 increase in liver volume relative to embryo volume from E8.5-E18, (**Figure 4A)** and an 8.7 x 10^4-fold increase in liver volume from E8.5 to E18 (**Figure 4B).** Interestingly, we identified previously unrecognized rapid bursts of growth between E8.5-E9.0, and E10 to E10.5, and E12 to E13 in both plots (**Figures 4A-B**). These bursts of growth were discontinuous and in 3 phases. There was only a 2-fold increase in liver bud volume between E9.0 and E10.0, but there was a 12.6-fold increase from E8.5 to E10.0, indicating discontinuous growth. Similarly, from E10.0-E11.5 we measured a 39.6-fold increase in volume, while there was only 1.4-fold increase between E10.5-E11.5. Further, between E12 and E18, we observed a 113,113-fold increase, but most of the changes occurred between E12 to E13 (1919.5-fold increase). We also calculated increases in surface area over time (**Figure 4C**) and cell number (**Figure 4D**) which followed similar trends. Overall, we observed discontinuous but rapid liver bud growth between E8.5-E18.

3D imaging of STM-epithelial interactions during murine liver bud development

We aimed to visualize the 3D STM and its relationship to the underlying 3D liver epithelium. Visualization of the STM at E8.5 demonstrates that it covers the inferior ~ ½ of the E8.5 liver bud (**Figure 5A, Supplemental Video 6)**. Interestingly, we find that the STM extends more ventrally for a

distance similar to the dorso-ventral thickness of the liver bud when viewed laterally (**Figure 5B, Supplemental Video 6).** The width of the STM in the lateral direction is about ¾ of the lateral thickness of the liver bud (**Figure 5A, 5C, Supplemental Video 6).** In the elliptically-shaped liver bud at E9.0 (**Figures 5D and 5E, Supplemental Video 7**), the STM extends laterally for a length equal to ¾ times the lateral (smaller) diameter, and covers approximately 80% of the liver bud. The caudal view of the E9.0 liver bud demonstrates how the STM contacts it directly (**Figures 5F, Supplemental Video 7**). At E9.5, the STM extends laterally about ½ times the diameter of the liver bud, and fully surrounds the liver bud. This suggests that the STM grows, remodels with the liver bud, and potentially primes the liver for growth (**Figures 5G-I, Supplemental Video 8**). At E9.5, the STM appears to be as thick as the liver bud when viewed laterally (**Figure 5H, Supplemental Video 9**), and when viewed in the ventral direction, the STM extends laterally, for a distance of 1/3 times the lateral width of the liver bud (**Figures 5I, Supplemental Videos 8-9**). At E10.0, compared to E9.5, the lateral STM thickness has increased (**compare Figure 5G and 5J**), the STM has diminished in the ventral direction (**compare Figure 5H to 5K**), and in the lateral direction (**compare Figure 5I to 5L**). We again quantified the relative and absolute growth of the STM. We observed an 8.8 x 10^2-fold increase in STM volume, as compared to 8.06 x 10^2-fold increase in liver bud volume over the same time period. Overall, the data demonstrated that the STM grows discontinuously, but mirrors the growth pattern of the mouse liver bud (**Figure 6A-B**), continues to envelope the liver bud with time, and extends ventrally and laterally through E10.0.

3D imaging of migrating cords and sheet-like growth in the developing human liver bud.

We retrieved data from the 3D Atlas of Human Embryology and 3D imaging of the human embryo in days 25, 28 and 33, which correspond to approximately E9.0, E10.5, and E11.5 in the mouse, respectively (*40*). Imaging of the 3D reconstructed liver demonstrates extensive lateral growth on days 28 and 33 (Supplementary **Figure 6A-C)**, and by day 33, we found that the liver epithelium (green) was indistinguishable from the STM (Supplementary **Figure 6C**). The day 25 liver bud demonstrates numerous cellular projections consistent with hepatic cords in multiple directions (**Figures 6A-6B, Supplemental Videos 10-11**). Interestingly, we again notice here not only narrow hepatic cords, but also prominent sheet-like structures at multiple levels, particularly visible in antero-lateral-inferior and antero-lateral-superior views (**Figures 6C-6D**). These cords and sheets continue to be present at Day 28 (**Figures 6E-H, Supplemental Videos 12-13**) in multiple views, with a large sheet present in the ventral direction (**Figure 6G**) with clear layering or stacking of sheet-like projections (**Figure 6H**). By Day 33, the liver surface has smoothened and greatly enlarged (**Figures 6I-J, Supplementary Figures 7-8, Supplemental Videos 14-15**). At this time, the liver demonstrates a 3D ellipsoid shape with a lateral axis of ~3500 µm and ~1000 µm in the cranial/caudal direction, indicating extensive lateral growth. We imaged inside the

3D reconstructed liver to analyze interconnections, and observed portions of the liver in enclosed spaces, which appear as green as enclosed spaces (**Figure 6K, Supplementary Videos 16**).

We quantified liver growth between day 25 and day 56 corresponding from E9.0 to E14 in the mouse. Interestingly, the absolute values of the measured volume at E9 and day 25 were 8.87 x 10^6 μm^3 and 1.4 x 10^6 μm^3 respectively. At E14 and day 56, absolute values of growth were 2.23 x 10^{11} and 1.05 x 10^{10} μm^3, respectively (**Figure 6I**). Analysis of human liver growth demonstrates discontinuous growth with short rapid increases. The data demonstrates 2.5 x 10^4–fold change in volume between day 25 and day 56, which is greater than the 7.5 x 10^3 change we measure from E9-E14 during mouse development (**Compare Figure 6I with Figure 3B**). Overall, the data demonstrates linear growth between days 25-33, and minimal growth on days 37-44, and 50-52 with burst of growth days 50 and 56.

3D imaging of STM-epithelial interactions during human liver bud development

We reconstructed the liver bud together with STM to image their interactions. Interestingly, the human liver bud was completely surrounded by STM on anterior, anterior-lateral, lateral, and posterior views. On Day 25, the lateral directions, the STM width is about ½ times the width of the liver in each direction, with the anatomical right side wider than the left (**Figures 7A-B, Supplemental Videos 17-18**). In the lateral view, the STM extends about ½ times the liver height, and about 1 times the liver height below (**Figure 7C).** Ventrally, the STM extends about ½ times the ventral distance of liver (**Figure 7C**). In the posterior and inferior views, the STM does not cover the posterior surface of the liver, but all the other surfaces are covered (**Figure 7D-E).**

On Day 28, the anterior view demonstrates that the STM has already been incorporated in to the liver laterally (**Figure 7F, Supplemental Videos 19-20)**. The lateral view demonstrates that the right lateral surface of the liver, posterior surface, and parts of the ventral surface are no longer interacting with STM (**Figure 7G)**. However, in the superior view along the gut tube, the STM still covers the liver. However, the thickness of the STM is approximately 100 μm (**Figure 7H)**. We quantified the STM growth compared to the liver growth at Day 25 and Day 28. The STM size increased by 0.54-fold, while the liver increased by 6.8-fold **(Figure 7I**).

DISCUSSION

Scientists are particularly interested in modeling liver organogenesis *in vivo* for disease modeling and therapeutic purposes. Organotypic cultures bearing cell types that are present in the fetal liver, with either primary (*42*) or stem cell-derived (*43*) cells, have demonstrated how liver organogenesis can motivate *in vivo* culture. A key question in liver regenerative medicine is, how does the fetal liver uniquely result in a

rapid, massive increase in size? To answer this, we focused on 3D dynamic imaging of hepatic cord formation, mesenchymal-liver epithelial interactions, and fetal liver growth in both mouse and humans. We used both the EMAP for mouse data and the 3D atlas of human embryology for human data, which enabled our approach. To image 3D liver bud morphogenesis at high spatial resolution, we performed 3D reconstructions of dynamic 2D imaging data. This enabled imaging both murine and human hepatic cords in 3D, for the first time, and comparison of structural differences. Our quantitative imaging and analysis of fetal liver growth showed that 3D fetal liver growth occurs in spurts rather continuously, with potential intermittent remodeling steps. Further, our analysis of the STM demonstrates that it increases in size during early fetal liver growth, that is highly interconnected with liver epithelium, and that it can have strong local effects on growth and remodeling. Finally, we identify and visualize human hepatic cord formation followed by rapid sheet-like growth, which we propose could be an under-appreciated morphological feature that enables rapid growth of early mouse and human fetal liver. These studies will motivate future improvement in organoid technology, *in vitro* culture, and human PSC differentiation for various application.

Fetal liver growth is unique and can be distinguished from liver regeneration from pre-existing HEPs. For example, fetal liver growth establishes the tissue architecture of the hepatic, biliary, and vascular components of the liver. Our data suggests that the mouse liver undergoes an overall 8.74×10^4-fold-increase in volume **(Figure 3B**) between E18 to E18, with small intermittent bursts when the liver bud is not remodeling. Further, we found a 7.5×10^3 change in volume from E9-E14, which corresponds to 2.5×10^4–fold change in volume between day 25 and day 56 in humans. In contrast, a recent study ultrasound study of human liver growth between days 126 to 210 (18 weeks to 30 weeks), demonstrated an approximate 7.3-fold increase in volume (*27*) over the 12 week time period. This suggests that exponential growth occurs early in liver development in mouse, while in humans an exponential phase is followed by a more linear phase, during the second and third trimester. These data are consistent with studies that demonstrate embryonic day 14 (E14) fetal rat HEPs are still proliferating after 6 months (or equivalent of 12 human years) with full rat liver repopulation (*44*). Consistent with this, E18 rat F-Heps or phenotypically isolated rat E19 fetal hepatic progenitors were shown more recently to repopulate ~1/3 the liver mass in acute models (*45*) and in chronic models (*46*), with evidence of coincident anti-inflammatory effects (*47*). Continued studies are needed to translate fetal liver repopulation to 3D liver organogenesis.

A key finding is that we report imaging of the 3D hepatic cords in humans and mice. Interestingly, we observe hepatic cords at an earlier stage in mice (E9.0) than previously reported (E9.5). This is likely because our technique has a higher spatial resolution than tissue sectioning and samples the entire tissue. However, natural variation may explain the differences in this data. Our 3D data agrees with

existing data and confirms that these cords migrate to form the trabeculated liver by E10.0. It remains to be determined how the 3D hepatic cords for the trabeculated liver, and this could be imaged by obtaining data at more time points after E9.5 and before E10.0. Our data suggests the human liver bud generally has more hepatic cords than the mouse, and more predominantly in the lateral directions. This could be because the liver grown even larger in humans, and lateral growth is a key mechanism. Further, we observed these hepatic cords merging into sheets in the human liver, prior to trabeculation, in both mouse and humans. We speculate that this additional "sheet morphogenesis" step may be critical for exponential growth which occurs in the mouse and human liver. Previous studies have used the term "sheet-like" growth in early fetal liver cultures (*48*), and the term HEP sheets has been used to describe mature liver architecture. While hepatic cords have been described to form hepatic sheets which flank the sinusoids, it is unclear if "sheet-like morphogenesis" has been imaged. From our images, it is also unclear if there are layers of mesenchyme between the observed sheets, which would be the interesting subject of a future study.

Our analysis demonstrates the importance of interactions between the emerging liver epithelium and the STM. Interestingly, our data indicates the murine STM grows during at a nearly identical rate to the liver bud between E8.5-E10, and the absolute volume of the STM slightly larger than that of the liver bud from E8-E10. These two facts are not obvious from the approach of traditional tissue sections. While STM expresses inductive signals like BMP, the expanding STM indicates the complex role of the STM, and potentially reciprocal signaling between the hepatic endoderm/hepatoblasts. This is consistent with the role of GATA6 and GATA4 within the STM, in which GATA6 and GATA4 knockout via tetraploid blastocyst complementation demonstrates loss of STM mass and inhibits early liver bud development (*21*) (*49*). Our analysis indicates that large portions of the STM are in a remote location from the liver bud, raising questions of what their role is, because of potential diffusion limitations. Further, human liver bud formation suggests that after sheet-like growth, the STM has been obliterated and internalized laterally, while not in the anterior directions. This strongly suggests the STM may play a role in sheet formation and incorporation of the STM into the liver (**Figure 9H**). However, we can only speculate regarding the mechanisms by which the STM may accomplish this. Another potential role of the STM is in contributing to liver bud remodeling, and not just growth.

There are several limitations to this study. One of the major weaknesses of our study was that there was only n=1 mouse for each time point analyzed in one stain of mice. The databases we used have between 1-4 mice for each condition tested, but only 1 data set per time point is available for download. A key limitation is also that we were some instances, particularly at later time points in the mouse and human, where there was some likely human error regarding segmentation. Our attempt to mitigate this was by having the same authors perform all the segmentation. Another issue is that using our approach,

one cannot distinguish between endothelial cells and blood vessels, STM, hematopoietic stem cells and their progeny, stellate cells, and immune cells, all of which have key roles in liver growth. Nonetheless, we have identified new aspects to liver growth, liver morphogenesis, and interactions between liver epithelium and STM. Newer techniques can be employed, like CT, MRI, photoacoustic imaging, and optical projection imaging, to improve datasets, and coupling 3D anatomical information to molecular information like gene expression, could be performed using techniques liked expansion microscopy (*50*). Another approach to understand these morphogenetic steps is whole embryo culture at the earliest stages. Overall, we feel understanding and imaging 3D these processes may lead to further insights in how the liver manages to greatly expand its mass while establishing an underlying complex architecture.

FIGURE LEGENDS

Figure 1. 3D reconstruction and visualization of the developing murine liver bud.

A) 3D reconstruction focused on the liver murine liver bud, at E8.5. Ventral view. A = anterior, V = ventral, P = posterior. Arrows depict directions, gut tube (yellow), the liver bud (green).
B) Same as A, except E9.0.
C) Same as B, except E9.5.
D) Same as C, except E10.0.

Figure 2. Multiple views of 3D murine liver bud demonstrate cord-like structures.

A) 3D reconstruction of the E9.0 murine liver bud. Ventral view. A = anterior, V = ventral, P = posterior. Arrows depict examples of migrating cords. Liver bud depicted in green.
B) Same as A), except dorsal view.
C) Same as B), except right lateral view. Arrows depict sheet-like growth at various levels from superior to inferior
D) 3D reconstruction of the E9.5 murine liver bud. Inferior view. A = anterior, V = ventral, P = posterior. Arrows depict hepatic cords. Liver bud depicted in green.
E) Same as B), except left lateral view.
F) 3D reconstruction of the E10.0 murine liver bud. Ventral view. A = anterior, V = ventral, P = posterior. Arrows depict examples of migrating cords. Liver bud depicted in green.
G) Same as C), except left lateral view.
H) Same as C), except inferior view.

Figure 3. Quantification of the volumetric growth and surface area of the murine developing liver.

A) Ratio of the reconstructed 3D liver murine liver growth compared to the mouse embryo at E8.5-E18. Bars are colored based on two major stages in liver development, embryonic E8.5-E11.5, and fetal stage E12-18.
B) Absolute volume of the reconstructed 3D liver murine liver growth at E8.5-E18. Bars are colored based on two major stages in liver development, embryonic E8.5-E11.5, and fetal stage E12-18.
C) Quantification of surface area during reconstructed 3D murine liver growth at E8.5-E18.
D) Quantification of the number of cells during reconstructed 3D murine liver growth at E8.5-E18.

Figure 4. Visualization of 3D reconstructed murine liver bud and septum transversum mesenchyme (STM) interactions.

A) 3D reconstruction of the liver murine liver bud and STM, at E8.5. Ventral view. Liver bud (green), STM (red)
B) Same as A) except right lateral view
C) Same as A) except inferior view
D) 3D reconstruction of the liver murine liver bud and STM, at E9.0 Superior, Ventral, lateral view. Liver bud (green), STM (red)
E) Same as D) except ventral, right lateral view
F) Same as E) except ventral, inferior view
G) 3D reconstruction of the liver murine liver bud and septum transversum mesenchyme, at E9.5 Ventral, lateral view. Liver bud (green), STM (red)
H) Same as G) except right lateral view
I) Same as G) except dorsal view
J) 3D reconstruction of the liver murine liver bud and STM, at E10.0 Ventral, lateral view. A = anterior, V = ventral, P = posterior. Arrows depict directions, the liver bud (green), STM (red)
K) Same as J) except left lateral view
L) Same as J) except posterior view

Figure 5. Quantification of septum transversum mesenchyme (STM) volume during murine liver development.

A) Ratio of the reconstructed 3D liver murine liver growth compared to the mouse embryo at E8.5-E10. Red =STM, Green = liver bud.

B) Absolute volume of the reconstructed 3D liver murine liver growth at E8.5-E10. Red =STM, Green = liver bud.

Figure 6. 3D reconstruction and visualization of the developing human liver bud.

A) 3D reconstruction focused of the human liver bud on day 25. Ventral, lateral view. A = anterior, V = ventral, P = posterior. Arrows depict migrating cords, gut tube (yellow), the liver bud (green).
B) Same as A) except ventral view.
C) Same as A) except, inferior, left lateral, ventral view.
D) Same as A) except, superior, left lateral, ventral view.
E) 3D reconstruction focused of the human liver bud on day 28. Ventral, lateral view. A = anterior, V = ventral, P = posterior. Arrows depict migrating cords, gut tube (yellow), the liver bud (green).
F) Same as E) except superior, dorsal view. Arrows depict cords forming cylindrically
G) Same as E) except ventral view. Arrows depicting sheets of migrating cells.
H) Same as E) except inferior view. Arrows depicting cords and sheets of migrating cells.
I) 3D reconstruction focused of the human liver bud on day 33. Ventral view. A = anterior, V = ventral, P = posterior.
J) Same as I) except lateral view.
K) Inside view of the 3D reconstruction focused of the human liver bud on day 33. The green images demonstrate numerous enclosed green structures all of which are in fact empty spaces within the 3D constructed liver.
L) Quantification of human liver bud volume during human liver development until Day 56 (8 weeks).

Figure 7. Visualization of 3D reconstructed human liver bud and septum transversum mesenchyme (STM) interactions.

A) 3D reconstruction of the liver murine liver bud and STM, at Day 25. Ventral view. Liver bud (green), STM (red)
B) Same as A, except superior, lateral view
C) Same as A, except right, lateral view
D) Same as D, except dorsal view
E) Same as A, except inferior view

F) 3D reconstruction of the liver murine liver bud and STM, at Day 28. Ventral lateral view. Liver bud (green), STM (red)

G) Same as A, except superior, lateral view

H) Same as A, except right, lateral view

I) Quantification of human STM and liver bud volume during human liver development on days 25 and 28.

SUPPLEMENTARY FIGURE LEGENDS

Supplemental Figure 1. Dynamic 3D imaging of murine liver development in whole embryo.

A) Coronal, black and white, hematoxylin and eosin (H+E) stain tissue section at E9.5 of mouse development, obtained from eMouseAtlas database, and corresponding segmented image. In segmented image, the gut tube (yellow), the liver bud (green) and STM (red) were segmented. A = Anterior, V = Ventral, P = Posterior, D= Dorsal. Arrows depict liver bud.

B) Same as A, except sagittal sections and corresponding segmented image.

C) Whole mouse embryo 3D reconstruction demonstrating reconstructed mouse on E8.5. Each tissue of interest was identified and thresholded and traced on individual, transverse tissue slices using known cross sectional anatomy and pre-identified labels within the database. Gut tube (yellow), the liver bud (green) and STM (red). A = anterior, V = ventral, P = posterior, D= Dorsal.

D) Same as C) except E9.0.

E) Same as D) except E9.5.

F) Same as E) except E10.0.

Supplemental Figure 2. Segmentation process of murine liver development in whole embryo at E8.5.

A) Coronal, black and white, hematoxylin and eosin (H+E) stain tissue section at E8.5 of mouse development, obtained from eMouseAtlas database, and corresponding segmented image. In segmented image, the gut tube (yellow), the liver bud (green) and STM (red) were segmented. A = Anterior, V = Ventral, P = Posterior, D= Dorsal. Arrows depict liver bud.

B) Same as A, except sagittal sections and corresponding segmented image.

Supplemental Figure 3. Segmentation process of murine liver development in whole embryo at E9.0.

Same as Supplemental Figure 2 except E9.0.

Supplemental Figure 4. Segmentation process of murine liver development in whole embryo at E10.0.

Same as Supplemental Figure 2 except E9.0.

Supplemental Figure 5. Sagittal view of developing murine liver at E8.5.

The liver bud (green) at the top left leads into the anterior direction of the gut tube and bottom right leads into the posterior.

Supplemental Figure 6. 3D reconstruction and visualization of human liver development in whole embryo.

A) Whole human embryo 3D reconstruction demonstrating reconstructed human embryo on Day 25. Each tissue of interest was identified and thresholded and traced on individual, transverse tissue slices using known cross sectional anatomy and pre-identified labels within the database. Gut tube (yellow), the liver bud (green) and STM (red). A = Anterior, V = Ventral, P = Posterior, D= Dorsal.
B) Same as A except Day 28 in human development.
C) Same as B except Day 33 in human development.

Supplemental Figure 7. Ventral view of human liver development at Day 33.

The liver bud (green) and gut tube (yellow) is viewed at the anterior position looking towards ventral. Scale in microns.

Supplemental Figure 8. Dorsal view of human liver development at Day 33.

Dorsal view of liver bud (green) and gut tube (yellow). Scale in microns.

Supplemental Video 1. Murine liver bud at E8.5 in 360° rotation through sagittal plane.

Ventral view of liver bud (green) rotating through sagittal plane. Units in axis are microns.

Supplemental Video 2. Murine liver bud at E9.0 in 360° rotation through sagittal plane.

Ventral view of liver bud (green) rotating through sagittal plane. Units in axis are microns.

Supplemental Video 3. Murine liver bud at E9.5 in 360° rotation through sagittal plane.

Ventral view of liver bud (green) rotating through sagittal plane. Units in axis are microns.

Supplemental Video 4. Murine liver bud at E10.0 in 360° rotation through sagittal plane.

Ventral view of liver bud (green) rotating through sagittal plane. Units in axis are microns.

Supplemental Video 5. Interior view of murine liver bud at E10.0.

Interior view of liver bud (green) through sagittal plane. Interior view is inverted as the structures (green) are voids within the liver bud and empty space is where the liver bud is solid. Units in axis are microns.

Supplemental Video 6. Murine liver bud and STM at E8.5 in 360° rotation through sagittal plane.

Ventral view of liver bud (green) and STM (red) rotating through sagittal plane. Units in axis are microns.

Supplemental Video 7. Murine liver bud and STM at E9.0 in 360° rotation through sagittal plane.

Ventral view of liver bud (green) and STM (red) rotating through sagittal plane. Units in axis are microns.

Supplemental Video 8. Murine liver bud and STM at E9.5 in 360° rotation through sagittal plane.

Ventral view of liver bud (green) and STM (red) rotating through sagittal plane. Units in axis are microns.

Supplemental Video 9. Murine liver bud and STM at E10.0 in 360° rotation through sagittal plane.

Ventral view of liver bud (green) and STM (red) rotating through sagittal plane. Units in axis are microns.

Supplemental Video 10. Human liver bud at Day 25 in 360° rotation through sagittal plane.

Ventral view of liver bud (green) rotating through sagittal plane. Units in axis are microns.

Supplemental Video 11. Human liver bud at Day 25 in 360° rotation through sagittal plane.

Ventral view of liver bud (green) rotating through transverse plane. Units in axis are microns.

Supplemental Video 12. Human liver bud at Day 28 in 360° rotation through sagittal plane.

Ventral view of liver bud (green) rotating through sagittal plane. Units in axis are microns.

Supplemental Video 13. Human liver bud at Day 28 in 360° rotation through sagittal plane.

Ventral view of liver bud (green) rotating through transverse plane. Units in axis are microns.

Supplemental Video 14. Human liver bud at Day 33 in 360° rotation through sagittal plane.

Ventral view of liver bud (green) rotating through sagittal plane. Units in axis are microns.

Supplemental Video. 15. Human liver bud at Day 33 in 360° rotation through sagittal plane.

Ventral view of liver bud (green) rotating through transverse plane. Units in axis are microns.

Supplemental Video 16. Interior view of human liver bud at day 33.

Interior view of liver bud (green) through sagittal plane. Interior view is inverted as the structures (green) are voids within the liver bud and empty space is where the liver bud is solid. Units in axis are microns.

Supplemental Video 17. Human liver bud and STM at Day 25 in 360° rotation through sagittal plane.

Ventral view of liver bud (green) and STM (red) rotating through sagittal plane. Units in axis are microns.

Supplemental Video 18. Human liver bud and STM at Day 25 in 360° rotation through sagittal plane.

Ventral view of liver bud (green) and STM (red) rotating through transverse plane. Units in axis are microns.

Supplemental Video 19. Human liver bud and STM at Day 28 in 360° rotation through sagittal plane.

Ventral view of liver bud (green) and STM (red) rotating through sagittal plane. Units in axis are microns.

Supplemental Video 20. Human liver bud and STM at Day 28 in 360° rotation through sagittal plane.

Ventral view of liver bud (green) and STM (red) rotating through transverse plane. Units in axis are microns.

ACKNOWLEDGEMENTS:

NP was supported by University at Buffalo, School of Engineering, State University of NY startup funds and University at Buffalo, State University of NY, Stem cells and Regenerative Medicine program (ScIRM)", (New York Stem Cell Science NYSTEM (Contract #C30290GG). OO was supported by the Western New York Prosperity Fellowship.

AUTHOR CONTRIBUTIONS:

TM: Obtained data, analyzed data, developed methodology for acquisition and analysis, wrote and approved manuscript.

OO: Obtained data, analyzed data, developed methodology for acquisition and analysis, wrote and approved manuscript.

CS: Obtained data, analyzed data, approved manuscript

SR: Obtained data, analyzed data, approved manuscript

SR: Obtained data, analyzed data, approved manuscript

NP: Conceptualized, acquired funding, investigated, supervised, wrote, edited manuscript, and approved manuscript.

REFERENCES

1. O. Ogoke, J. Oluwole, N. Parashurama, Bioengineering considerations in liver regenerative medicine. *J Biol Eng* **11**, 46 (2017).
2. A. M. Zorn, in *StemBook*. (Cambridge (MA), 2008).
3. K. Si-Tayeb, F. P. Lemaigre, S. A. Duncan, Organogenesis and development of the liver. *Dev Cell* **18**, 175-189 (2010).
4. N. Ledouarin, [Induction of Prehepatic Endoderm by Mesoderm of the Cardiac Region in the Chick Embryo.]. *Journal of embryology and experimental morphology* **12**, 651-664 (1964).
5. R. Gualdi *et al.*, Hepatic specification of the gut endoderm in vitro: cell signaling and transcriptional control. *Genes & development* **10**, 1670-1682 (1996).
6. J. M. Rossi, N. R. Dunn, B. L. Hogan, K. S. Zaret, Distinct mesodermal signals, including BMPs from the septum transversum mesenchyme, are required in combination for hepatogenesis from the endoderm. *Genes Dev* **15**, 1998-2009 (2001).
7. K. Matsumoto, H. Yoshitomi, J. Rossant, K. S. Zaret, Liver organogenesis promoted by endothelial cells prior to vascular function. *Science* **294**, 559-563 (2001).
8. C. S. Lee, J. R. Friedman, J. T. Fulmer, K. H. Kaestner, The initiation of liver development is dependent on Foxa transcription factors. *Nature* **435**, 944-947 (2005).

9. R. Bort, M. Signore, K. Tremblay, J. P. M. Barbera, K. S. Zaret, Hex homeobox gene controls the transition of the endoderm to a pseudostratified, cell emergent epithelium for liver bud development. *Developmental Biology* **290**, 44-56 (2006).
10. H. Enzan *et al.*, Development of hepatic sinusoidal structure with special reference to the Ito cells. *Microsc Res Tech* **39**, 336-349 (1997).
11. J. P. Martinez Barbera *et al.*, The homeobox gene Hex is required in definitive endodermal tissues for normal forebrain, liver and thyroid formation. *Development* **127**, 2433-2445 (2000).
12. B. Sosa-Pineda, J. T. Wigle, G. Oliver, Hepatocyte migration during liver development requires Prox1. *Nat Genet* **25**, 254-255 (2000).
13. T. H. Ludtke, V. M. Christoffels, M. Petry, A. Kispert, Tbx3 promotes liver bud expansion during mouse development by suppression of cholangiocyte differentiation. *Hepatology* **49**, 969-978 (2009).
14. R. Bort, M. Signore, K. Tremblay, J. P. Martinez Barbera, K. S. Zaret, Hex homeobox gene controls the transition of the endoderm to a pseudostratified, cell emergent epithelium for liver bud development. *Dev Biol* **290**, 44-56 (2006).
15. S. Cascio, K. S. Zaret, Hepatocyte differentiation initiates during endodermal-mesenchymal interactions prior to liver formation. *Development* **113**, 217-225 (1991).
16. T. Suzuki *et al.*, Crucial role of the small GTPase ARF6 in hepatic cord formation during liver development. *Mol Cell Biol* **26**, 6149-6156 (2006).
17. M. Weinstein *et al.*, Smad proteins and hepatocyte growth factor control parallel regulatory pathways that converge on beta1-integrin to promote normal liver development. *Mol Cell Biol* **21**, 5122-5131 (2001).
18. N. Tatsumi, R. Miki, K. Katsu, Y. Yokouchi, Neurturin-GFRalpha2 signaling controls liver bud migration along the ductus venosus in the chick embryo. *Dev Biol* **307**, 14-28 (2007).
19. C. Schmidt *et al.*, Scatter factor/hepatocyte growth factor is essential for liver development. *Nature* **373**, 699-702 (1995).
20. J. Cayuso *et al.*, EphrinB1/EphB3b Coordinate Bidirectional Epithelial-Mesenchymal Interactions Controlling Liver Morphogenesis and Laterality. *Dev Cell* **39**, 316-328 (2016).
21. A. J. Watt, R. Zhao, J. Li, S. A. Duncan, Development of the mammalian liver and ventral pancreas is dependent on GATA4. *BMC Dev Biol* **7**, 37 (2007).
22. T. J. Lints, L. Hartley, L. M. Parsons, R. P. Harvey, Mesoderm-specific expression of the divergent homeobox gene Hlx during murine embryogenesis. *Dev Dyn* **205**, 457-470 (1996).
23. H. Yagi *et al.*, Growth disturbance in fetal liver hematopoiesis of Mll-mutant mice. *Blood* **92**, 108-117 (1998).
24. A. Yoshimura *et al.*, Mouse oncostatin M: an immediate early gene induced by multiple cytokines through the JAK-STAT5 pathway. *EMBO J* **15**, 1055-1063 (1996).
25. S. Collardeau-Frachon, J. Y. Scoazec, Vascular development and differentiation during human liver organogenesis. *Anat Rec (Hoboken)* **291**, 614-627 (2008).
26. J. LeCouter *et al.*, Angiogenesis-independent endothelial protection of liver: role of VEGFR-1. *Science* **299**, 890-893 (2003).
27. M. Szpinda *et al.*, Three-dimensional growth dynamics of the liver in the human fetus. *Surg Radiol Anat* **37**, 439-448 (2015).

28. G. Pardi, I. Cetin, Human fetal growth and organ development: 50 years of discoveries. *Am J Obstet Gynecol* **194**, 1088-1099 (2006).
29. B. J. Nieman, M. D. Wong, R. M. Henkelman, Genes into geometry: imaging for mouse development in 3D. *Curr Opin Genet Dev* **21**, 638-646 (2011).
30. R. S. Udan, V. G. Piazza, C. W. Hsu, A. K. Hadjantonakis, M. E. Dickinson, Quantitative imaging of cell dynamics in mouse embryos using light-sheet microscopy. *Development* **141**, 4406-4414 (2014).
31. C. K. Phoon, Imaging tools for the developmental biologist: ultrasound biomicroscopy of mouse embryonic development. *Pediatr Res* **60**, 14-21 (2006).
32. S. H. Syed, K. V. Larin, M. E. Dickinson, I. V. Larina, Optical coherence tomography for high-resolution imaging of mouse development in utero. *J Biomed Opt* **16**, 046004 (2011).
33. M. D. Wong *et al.*, 4D atlas of the mouse embryo for precise morphological staging. *Development* **142**, 3583-3591 (2015).
34. D. H. Turnbull, S. Mori, MRI in mouse developmental biology. *NMR Biomed* **20**, 265-274 (2007).
35. M. Willadsen, M. Chaise, I. Yarovoy, A. Q. Zhang, N. Parashurama, Engineering molecular imaging strategies for regenerative medicine. *Bioeng Transl Med* **3**, 232-255 (2018).
36. H. Lickert *et al.*, Baf60c is essential for function of BAF chromatin remodelling complexes in heart development. *Nature* **432**, 107-112 (2004).
37. R. Baldock, J. Bard, M. Kaufman, D. Davidson, A real mouse for your computer. *Bioessays* **14**, 501-502 (1992).
38. B. S. de Bakker *et al.*, An interactive three-dimensional digital atlas and quantitative database of human development. *Science* **354**, (2016).
39. L. Richardson *et al.*, EMAGE mouse embryo spatial gene expression database: 2014 update. *Nucleic Acids Res* **42**, D835-844 (2014).
40. B. S. de Bakker, K. H. de Jong, J. Hagoort, R. J. Oostra, A. F. Moorman, Towards a 3-dimensional atlas of the developing human embryo: the Amsterdam experience. *Reprod Toxicol* **34**, 225-236 (2012).
41. R. I. Sherwood, T. Y. Chen, D. A. Melton, Transcriptional dynamics of endodermal organ formation. *Dev Dyn* **238**, 29-42 (2009).
42. M. E. Fomin, A. I. Beyer, M. O. Muench, Human fetal liver cultures support multiple cell lineages that can engraft immunodeficient mice. *Open Biol* **7**, (2017).
43. P. Guye *et al.*, Genetically engineering self-organization of human pluripotent stem cells into a liver bud-like tissue using Gata6. *Nat Commun* **7**, 10243 (2016).
44. M. D. Dabeva *et al.*, Proliferation and differentiation of fetal liver epithelial progenitor cells after transplantation into adult rat liver. *Am J Pathol* **156**, 2017-2031 (2000).
45. J. M. Boylan, H. Francois-Vaughan, P. A. Gruppuso, J. A. Sanders, Engraftment and Repopulation Potential of Late Gestation Fetal Rat Hepatocytes. *Transplantation* **101**, 2349-2359 (2017).
46. W. T. Bin, L. M. Ma, Q. Xu, X. L. Shi, Embryonic hepatocyte transplantation for hepatic cirrhosis: efficacy and mechanism of action. *World J Gastroenterol* **18**, 309-322 (2012).
47. M. I. Yovchev, Y. Xue, D. A. Shafritz, J. Locker, M. Oertel, Repopulation of the fibrotic/cirrhotic rat liver by transplanted hepatic stem/progenitor cells and mature hepatocytes. *Hepatology* **59**, 284-295 (2014).

48. S. Z. Hussain *et al.*, Wnt impacts growth and differentiation in ex vivo liver development. *Exp Cell Res* **292**, 157-169 (2004).
49. R. Zhao *et al.*, GATA6 is essential for embryonic development of the liver but dispensable for early heart formation. *Mol Cell Biol* **25**, 2622-2631 (2005).
50. F. Chen, P. W. Tillberg, E. S. Boyden, Optical imaging. Expansion microscopy. *Science* **347**, 543-548 (2015).

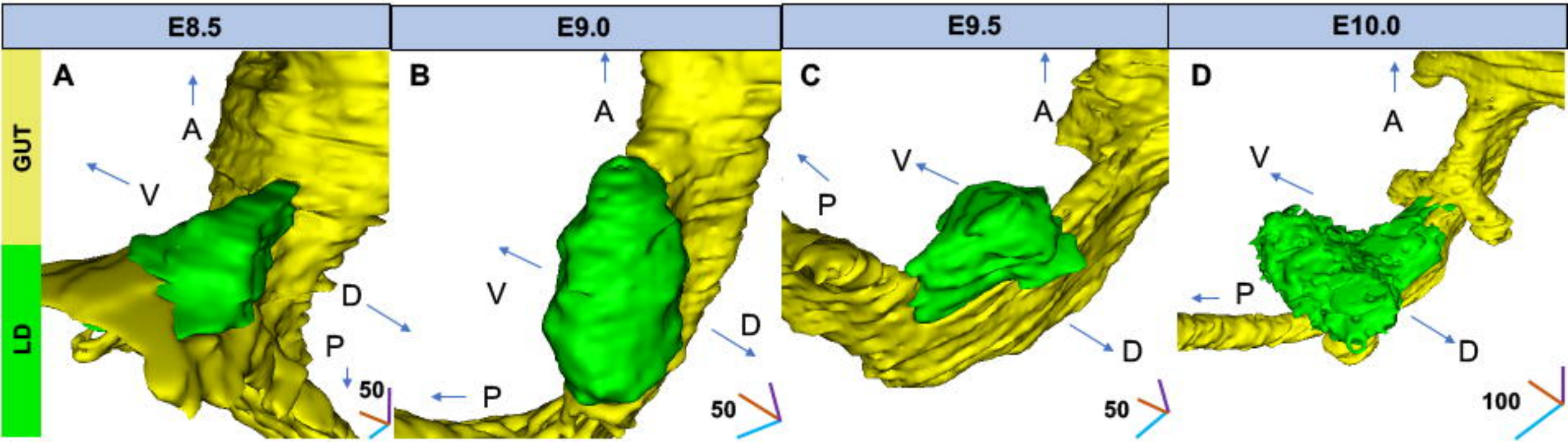
E8.5
E9.0
E9.5
E10.0
GUT
LD
A
V
D
P
50
100

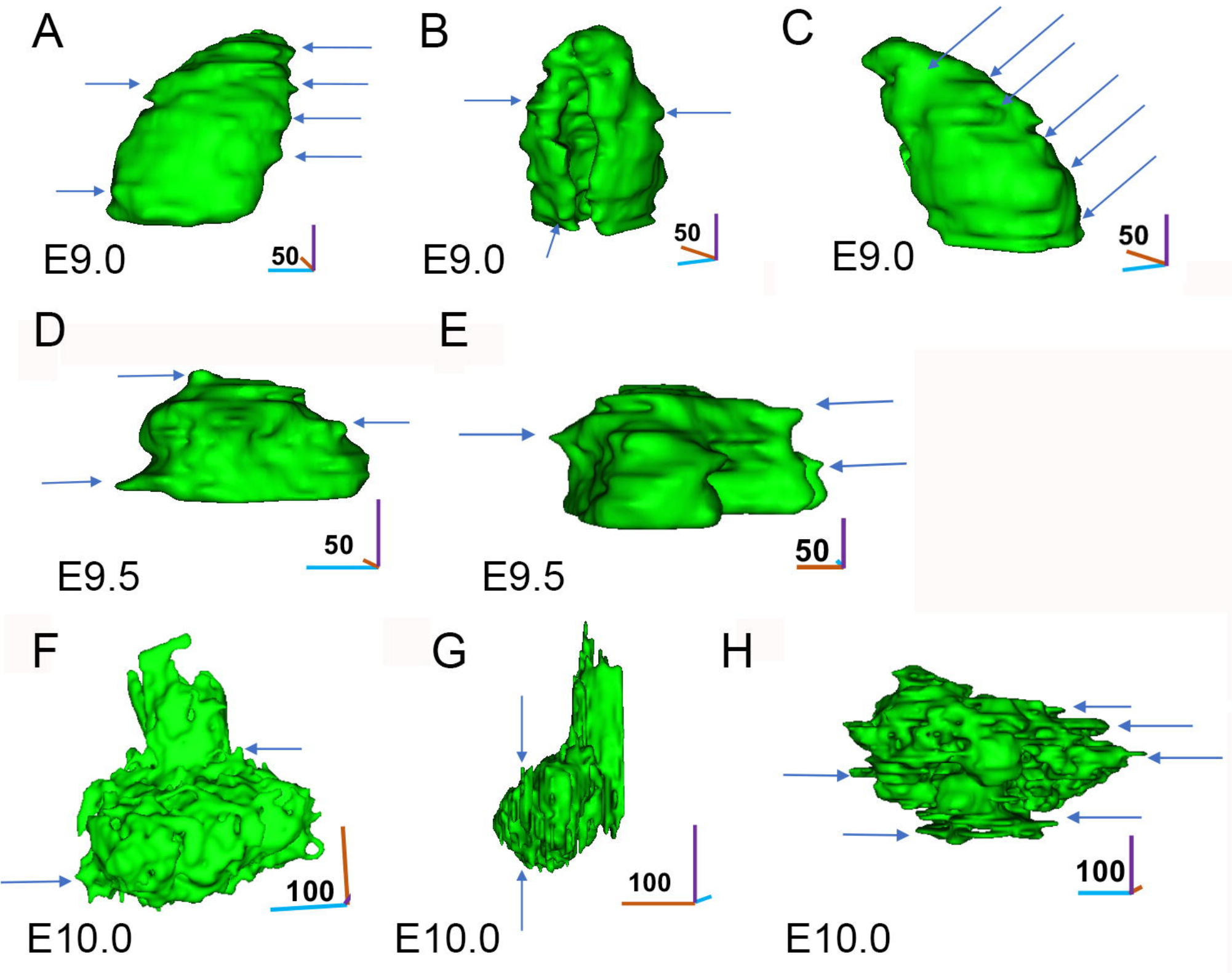
A
E9.0
50
B
E9.0
50
C
E9.0
50
D
E9.5
50
E
E9.5
50
F
E10.0
100
G
E10.0
100
H
E10.0
100

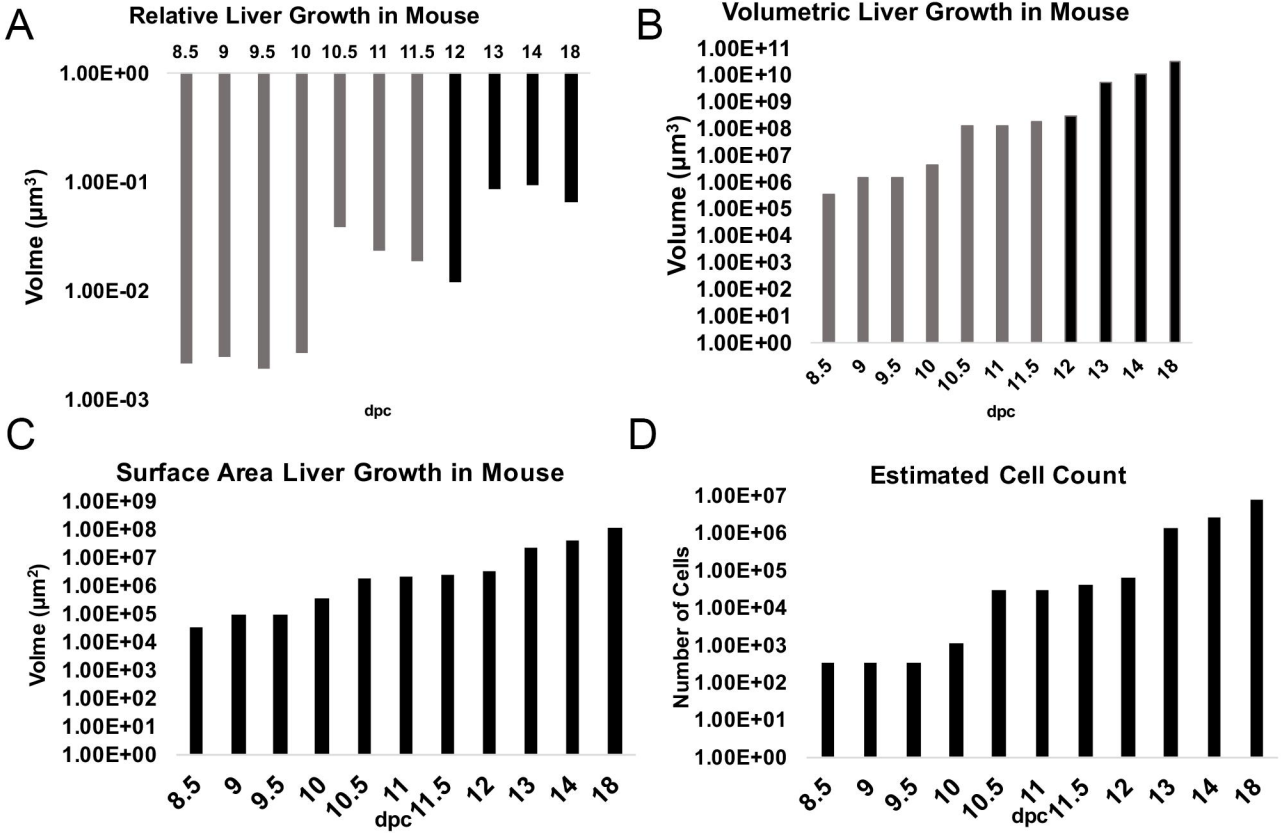
A
Relative Liver Growth in Mouse
8.5 9 9.5 10 10.5 11 11.5 12 13 14 18
1.00E+00
1.00E-01
1.00E-02
1.00E-03
Volme (µm³)
dpc
B
Volumetric Liver Growth in Mouse
1.00E+11
1.00E+10
1.00E+09
1.00E+08
1.00E+07
1.00E+06
1.00E+05
1.00E+04
1.00E+03
1.00E+02
1.00E+01
1.00E+00
Volume (µm³)
8.5 9 9.5 10 10.5 11 11.5 12 13 14 18
dpc
C
Surface Area Liver Growth in Mouse
1.00E+09
1.00E+08
1.00E+07
1.00E+06
1.00E+05
1.00E+04
1.00E+03
1.00E+02
1.00E+01
1.00E+00
Volme (µm²)
8.5 9 9.5 10 10.5 11 11.5 12 13 14 18
dpc
D
Estimated Cell Count
1.00E+07
1.00E+06
1.00E+05
1.00E+04
1.00E+03
1.00E+02
1.00E+01
1.00E+00
Number of Cells
8.5 9 9.5 10 10.5 11 11.5 12 13 14 18
dpc

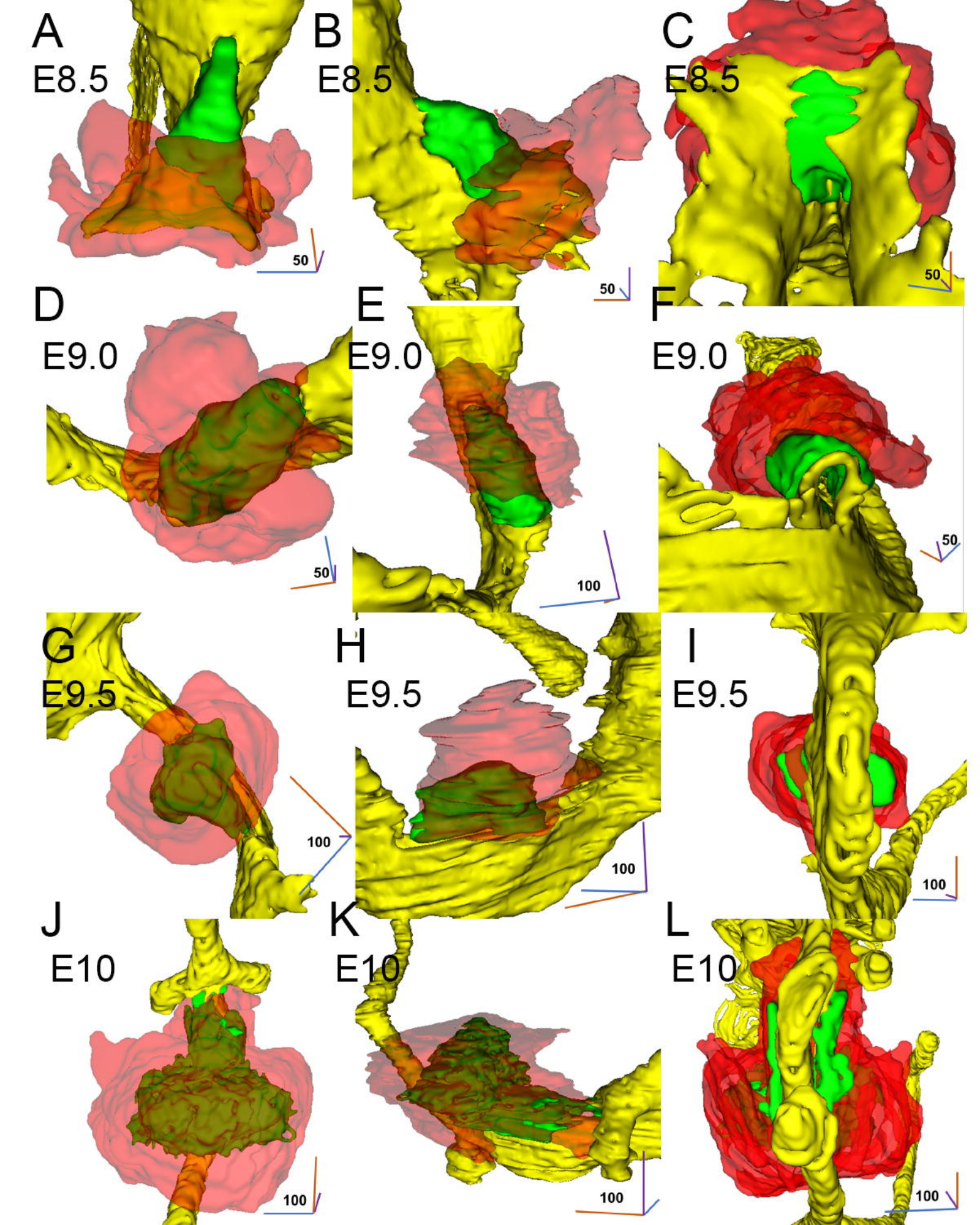
A
E8.5
50
B
E8.5
50
C
E8.5
50
D
E9.0
50
E
E9.0
100
F
E9.0
50
G
E9.5
100
H
E9.5
100
I
E9.5
100
J
E10
100
K
E10
100
L
E10
100

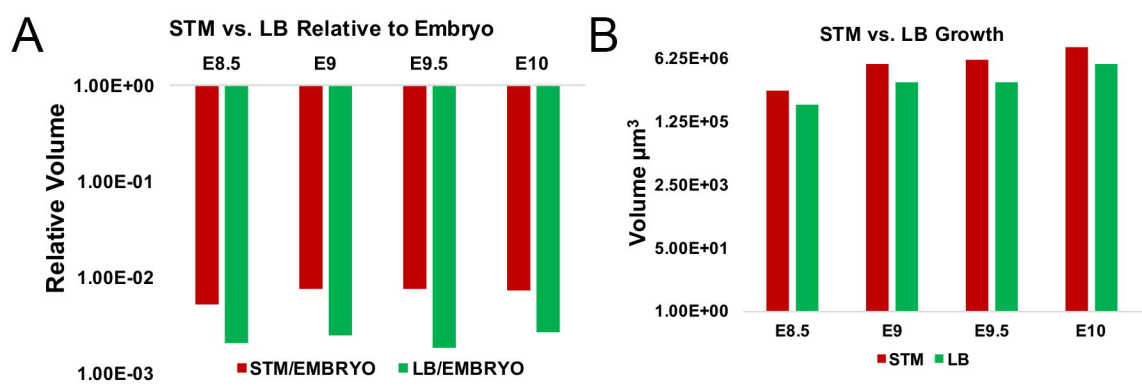
A
STM vs. LB Relative to Embryo
E8.5
E9
E9.5
E10
1.00E+00
1.00E-01
1.00E-02
1.00E-03
Relative Volume
STM/EMBRYO
LB/EMBRYO
B
STM vs. LB Growth
6.25E+06
1.25E+05
2.50E+03
5.00E+01
1.00E+00
Volume µm3
E8.5
E9
E9.5
E10
STM
LB

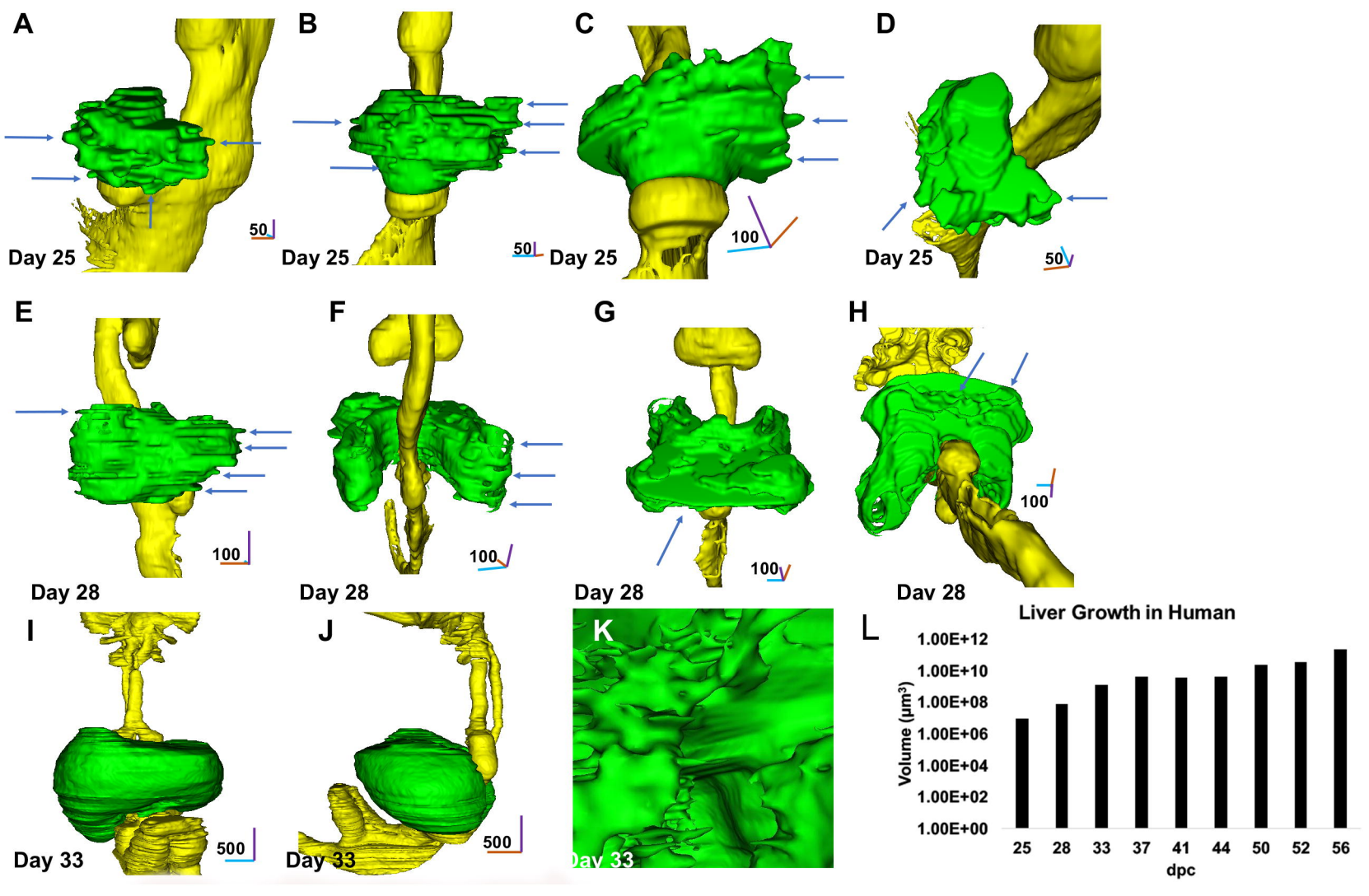
A
Day 25
50
B
Day 25
50
C
Day 25
100
D
Day 25
50
E
100
Day 28
F
100
Day 28
G
100
Day 28
H
100
Dav 28
I
Day 33
500
J
Day 33
500
K
Day 33
L
Liver Growth in Human
Volume (µm³)
1.00E+12
1.00E+10
1.00E+08
1.00E+06
1.00E+04
1.00E+02
1.00E+00
25
28
33
37
41
44
50
52
56
dpc